



Mauritius Research Council
INNOVATION FOR TECHNOLOGY

**EXPERIMENTAL
EVALUATION OF AN
EVACUATED TUBE SOLAR-
THERMAL COLLECTOR
MODEL**

Final Report

November 2017

Mauritius Research Council

Address:

Level 6, Ebene Heights
34, Cybercity
Ebene

Telephone: (230) 465 1235
Fax: (230) 465 1239
e-mail: mrc@intnet.mu
Website: www.mrc.org.mu

This report is based on work supported by the Mauritius Research Council under award number MRC/RSS-1704. Any opinions, findings, recommendations and conclusions expressed herein are the author's and do not necessarily reflect those of the Council.

University of Mauritius

**‘Experimental Evaluation of an
Evacuated Tube Solar-Thermal
Collector Model’**

Funded by Mauritius Research Council

Project Reference: MRC/RSS-1704

November 2017

Acknowledgement

This research study has been made possible through funding from Mauritius Research Council. Gratitude is extended to the Laboratory Officer of the Thermodynamics Lab, Mr D Goburdhun for providing assistance with equipment installation and usage.

Composition of the Research Team

The following academics of the University of Mauritius were involved in this project:

1. Dr Abdel Khoodaruth – Mechanical and Production Engineering Department.
2. Mr Vishwamitra Oree – Electrical and Electronic Engineering Department.
3. Mr Anshu Prakash Murdan – Electrical and Electronic Engineering Department.

A Research Assistant, Mr A Soopee, was recruited in connection to this project for a period of two months. The letter of appointment is enclosed (Appendix A).

Executive Summary

The main aim of this study is to design an evacuated tube solar water collector model for the correct prediction of its performance under different climate conditions and materials used for its manufacture. The ultimate objective is to develop a model that can be used to support the local SWH industry to optimize the performance of solar water heater. An experimental rig was set up with the installation requirements in accordance with ISO 9806:2013. The results were recorded over a fortnight, from which a selection of 3 hours was considered for validating a numerical thermal model, which can be adapted to the changing climatic conditions of Mauritius. The Boussinesq's approximation was employed for developing the numerical thermal model. A close agreement was met for the validation, with only a maximum of 2.06% deviation from experimental data. The temperature contours demonstrated that temperature within the water tank is quite uniform, with 5.0°C increase for each hour. An overall thermal efficiency of 40.39% was noted during the 3-hour solar exposure. It was also observed that the thermal efficiency undergoes very low (if not negligible) increases for solar irradiance values above 750 W/m². Furthermore, changes in thermal efficiency were found to follow any drastic fluctuations in solar irradiance, before stabilizing around 40.05% again.

Table of Contents

Acknowledgement	2
Executive Summary.....	4
Table of Contents	Error! Bookmark not defined.
1. Introduction	6
2. Project Schedule	9
3. Composition of the Research Team.....	3
4. Literature Review.....	9
4.1. Solar thermal collectors	9
4.2. Evacuated tube solar collector (ETSC)	10
4.3. Performance of Water-in-Glass ETSCs.....	11
5. Experimental Setup.....	12
6. Numerical Model	14
6.1. Governing Equations.....	14
6.2. Domain Discretization.....	15
6.3. Boundary and Initial Conditions.....	16
6.4. Experimental Data and Validation	17
7. Results and Discussions	19
7.1. Validation of Numerical Model.....	19
7.2. Temperature Fields.....	20
7.3. Thermal Efficiency of SWH.....	20
7.4. Effect of Tube Diameter on Thermal Efficiency	23
7.5. Effect of Climatic Conditions on Thermal Efficiency	24
8. Conclusion.....	26
References	27
Appendix A.....	Error! Bookmark not defined.
Appendix B.....	30

1. Introduction

With the alarming increase in greenhouse gas (GHG) in our atmosphere, and the depleting fossil fuel reserve, the need to develop methods of exploiting other cleaner and renewable energy resources is becoming more imperative. Around 24% of the world's total energy demand is currently being contributed by renewable energy sources, amounting to an increase of 22% over the last two decades [1].

Solar energy is amongst the cleanest forms of renewable energy, available cost-free for a wide range of the energy market demand. The earth's surface is exposed to 1.5×10^{18} kWh of solar energy incident throughout a year, which is 10,000 more than the entire world's annual energy consumption [2]. Because of its accessibility, availability, capacity, and efficiency as compared to other renewable energy sources, even in countries less likely to be favourable to use solar energy, numerous research activities are being invested into to further develop the technologies of solar energy capture. The applications of solar energy cover a wide range of the energy market: some examples are in building integration, for agricultural purposes, for heating and cooling, for desalination and wastewater treatment processes, and the space industry. Despite the contributing efforts of the scientific, governmental, and corporate entities in mitigating our energy reliance from fossil fuels to renewable resources and the considerable advancements in solar technology, there are still some barriers that are to be overcome [3, 4]. One of the main limiting barriers is the available daytime, particularly during winter seasons. However, a review study by Mussard *et al.* [5] has shown that even in those severe cold conditions, solar energy, as a standalone or hybrid system, can still be an efficient reliable alternative to fossil fuels for heating and cooling.

The geographical location of Mauritius benefits the country with around 6.5 to 8 hours of bright sunshine during the summer, and 5.0 to 7.5 hours during the winter, for high grounds and coastal regions respectively [6]. In 2014, the percentage of electricity generated by renewable sources in Mauritius is 22.7%, of which 3.82% by solar energy. A 2.0% of total power generation from solar energy is forecasted for 2025 [7]. In 2012, a recorded number of 35,000 solar water-heating units were installed in Mauritius, which represented an 8.0% penetration of the household market, as compared to 25,000 units in 2008 [7]. The purpose of the solar water heater (SWH) programme is to encourage the switch from electricity and gas to renewable energy. The 2008/2009 national

budget planned with Rs 250 million for a total of 25,000 applications - but the support scheme was more attractive than had been foreseen. The Maurice Ile Durable Fund, which was responsible for the administration of the programme, received 49,000 applications within one and a half years alone.

Grants are an important driver of the solar thermal market in Mauritius. Although, it is a sunny island, most Mauritian citizens will certainly like to have a solar system, but, unfortunately, many people cannot afford to buy one due to the relatively high costs involved. The Government launched a second phase of the Solar Water Heater Scheme, a Rs250 million worth programme financed by the Maurice Ile Durable Fund, was implemented since mid-January 2012 in collaboration with the Development Bank of Mauritius (DBM). It is expected that some 24 000 families benefitted from this scheme which aims at encouraging Mauritians to opt for renewable sources of energy and reduce the country's dependency on fossil fuels for the production of electricity. Under this scheme, Government gave a grant Rs 10,000 as subsidy for the purchase of solar water heaters. The grant of Rs 10,000 was re-activated last year.

Mauritius has 1.3 million inhabitants with about 325,000 households. According to Statistics Mauritius, 14% of the households have installed SWH. The percentage of SWH installed was of the range of 8-18%. It was found the penetration of SWH was higher in the north part of the island whereas in the south west part of the island, the penetration was only 9.0%. In fact, the topography of Mauritius is marked by coastal plains that gradually slope towards disjointed mountains encircling a central plateau. The wind regime consists of south-easterly trade winds that blow over the island during the year. Clouds predominantly reach the island by the southern coast and are blown by the trade winds. The high inland mountains block the clouds from progressing towards the northern part. As a result, the northern part of the island frequently enjoys clear sky days and the southern coast has less clear sky sunshine. However, no survey has been done for the high or low penetration of SWH in certain regions of the island.

With the different incentive schemes integrated by the government, the number is expected to increase over the years. Nevertheless, a target of 2.0% of solar power generation is not much of a value. Such a small percent of implementation can be attributed to the high initial capital investment that entails with mitigating to solar energy, the ideological scepticism over varying

climatic conditions, and its intermittent nature. However, recent developments have drastically reduced the cost of initial investment in solar photovoltaic (PV) technology (a reduction of greater than 80% over the past decade), while also boosting the output efficiency of solar technologies, which will definitely make solar energy integration more attractive [8]. Besides using photovoltaic cells for solar energy harvesting, the developments in solar-thermal collectors are quite substantial as well. The scope of this project will be focused on addressing the performance evaluation of evacuated tube solar collectors through experimental as well as numerical studies under the climatic conditions of Mauritius.

The aim of the project is therefore to design an evacuated tube solar water collector model for the correct prediction of its performance under different climate conditions and materials used for its manufacture. Furthermore, the objectives of the project are to use the evacuated tube solar water collector model as an optimization tool for a wide range of geometries and solar collector designs and to simulate the dynamic behaviour of the solar water collector under different climate conditions.

The methodology used to achieve the above mentioned objectives were as follows:

- Carry out literature review in the field of research.
- Setting up the prototype for carrying out the experiments.
- Devise thermal models for the solar-thermal collector and correlate to data collected on-site.
- An evacuated tube solar water collector test facility was set up. Research-standard equipment was used for the measurement and logging of temperature of water entering and leaving the solar collector and climatic data including ambient temperature, sunshine hours and solar radiation
- A model was developed with the help of a specialized software ANSYS and simulated for the actual location of the solar water collector
- The simulated results were compared with the real-time data.
- Once the model was validated, the performance of the solar water collector was simulated for the various climatic conditions and different geometries such as varying the diameter of the tube of the collector.

2. Project Schedule

The duration of the project was six months starting on 15 May 2017 and completed on 20 November 2017.

3. Literature Review

3.1. Solar thermal collectors

Solar thermal collectors are considered to be of better alternative than using PV panels in terms of efficiency in converting solar energy into a form that is directly useful for our consumption. However, both technologies are adequate to mitigate our energy reliability from fossil fuels. As far as it goes to small-scale building integration applications, solar thermal collectors are more appropriate for heating purposes as compared to PV panels, the latter being more suitable for electricity generation.

A solar thermal collector is a device that captures solar thermal energy through a specific absorbing material and transfer it to a working fluid, usually identified as the heat transfer fluid (HTF). The HTF will then in turn transfer the acquired heat energy to a second HTF (usually water or air) in a heat exchange. This results in two separate closed systems for the two HTFs as shown in Fig. 1. The performance of solar thermal collectors relies mostly on how efficient the HTFs can extract and carry the solar heat energy through its different networks. Hence the classifications of a solar collector performance are based on: the heat transfer coefficient of the absorber and HTFs, the coating material on the absorber, and the thermal conductivity of the HTFs and the piping network [9].

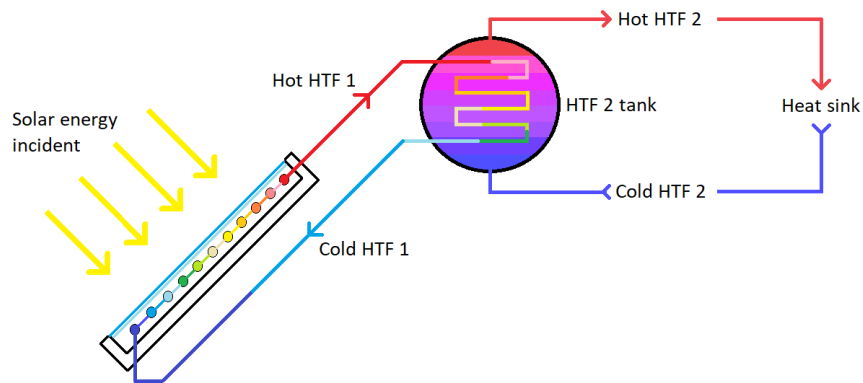


Figure 1 – Typical working principle of a solar thermal collector.

Typical values for thermal performance of solar collectors range from 20-80% [10-16], subjected to the solar collector type, configuration, and the ambient conditions. Using temperatures below ambient conditions, Bunea *et al.* [17] investigated the performance of four different solar collectors which produced results close to maximum theoretical values of thermal efficiency 80-95%. Solar thermal collectors can be classified into three different categories: non-tracking, one-axis tracking, and two-axes tracking. The non-tracking collectors have stationary solar collectors, namely flat plate, compound parabolic, and evacuated tube solar collectors (ETSCs) [9], of which the latter classification is relevant to this study.

3.2 Evacuated tube solar collector (ETSC)

Of the three stationary solar collectors mentioned, ETSCs are known to be most efficient [14], with the ability to absorb both, direct and diffuse radiations. ETSCs consist of two concentric glass tubes, in between which is a vacuum space, thereby drastically minimizing any convection heat loss. The outer tube glass entraps a vacuum chamber to minimize convective heat loss, with a selective absorber coating enveloping the inner glass tube for transmitting the absorbed solar energy to the HTF within (Figure 2a). And due to the cylindrical shape of the tubes, passive tracking of the sun is possible throughout the day, thus not limiting the period over which solar energy can be harnessed. This is the first step of solar energy transmission for ETSCs. From there on, the energy harnessing varies by design, splitting into two major categories: heat pipe and all-in-glass ETSCs. Considering the current ETSC installed at the University of Mauritius, our focus will be mainly on the less costly all-in-glass (water-in-glass) ETSC.

All-in-glass ETSCs operate on a basic principle known as thermosiphon, which is a buoyancy driven flow due to a difference in fluid density. With its cylindrical shape, the sun irradiance shining on the outer tube glass (Figure 2b) passes through the vacuum space to reach the selective absorber coating. The fluid in the upper half region of the inner glass is heated, causing a decrease in its density. Because of the higher fluid density in the lower half of the inner tube, a buoyant force causes motion of the fluid as depicted in Figure 2c. This phenomenon is known as the thermosiphon phenomenon. For this work, the fluid in consideration will be water.

3.3. Performance of Water-in-Glass ETSCs

The performance of water-in-glass ETSCs are mostly relevant and shows to be most efficient than other flat plate collectors for domestic applications as documented by the research work of Morrison *et al.* [18] for direct water heating. Zhang *et al.* [19] conducted experiments to determine optimum factors regarding the evacuated tube length and spacing, insulation material thickness, solar collector angle, and ratio of water tank length and solar collector area. The optimum values are described, bearing in mind that the experimental investigation was conducted for the climate conditions of Tianjin, China. Thant *et al.* [20] evaluated the temperature distribution in water-in-glass ETSC through a numerical model with variations in evacuated tube dimensions as well as their inclination. The work suggested better results for lower tilt angles and with a tube diameter-to-length ratio of 0.0261. However, these research studies focus mainly on the performance for transient operation of water-in-glass ETSCs. What will be of higher interest to this work is literature on water-in-glass ETSC performance during passive state, i.e. with no charge or discharge of water.

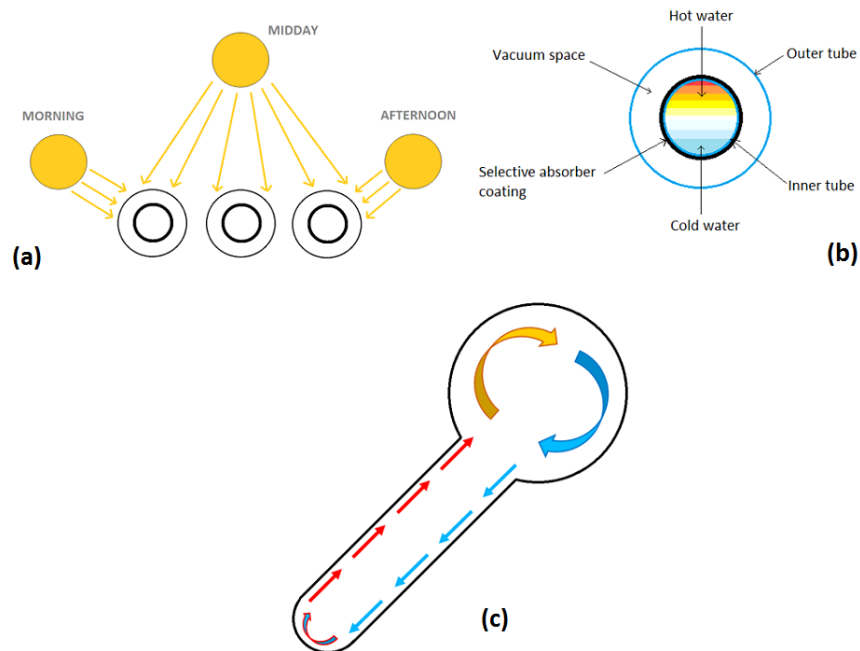


Figure 2 – (a): Passive tracking ability of ETSCs. (b): Cross-section of evacuated tube showing the two concentric glass tubes, with water within the inner tube. (c): Cross-section of a solar water heater showing the buoyant driven water flow due to the thermosiphon phenomenon

Several literatures can be found in that context to have investigated the performance of water-in-glass ETSCs with variations in parameters such as tilt angle of the evacuated tubes, working fluid, materials used, and water tank sizing of ETSCs. Thomas [21] conducted experimental as well as simulation investigations on the performance of water-in-glass ETCs with variations in tilt angle of the evacuated tubes. It was found that the optimum angle is around 10°. In a similar performance investigation, but by conducting passive experiments and simulations on an ETSC (i.e. with no water charge or discharge from the system), Bracamonte *et al.* [22] concluded that a 10° tilt angle produced higher temperature rise as well as thermal stratification within the water tank, with a thermal inactive region at the bottom of the tank. However, Bracamonte *et al.* [22] also documented that with higher tilt angles (around 45°), a more uniform mix of temperature was obtained, with lower thermal stratification. The position at which the evacuated tubes connect to the water tank as well was found to be of significance importance for thermal stratification within [23]. On a different line of thought, Tang *et al.* [24] performed similar investigations but during nocturnal times. It was established that during the night, water temperature inside the tubes were lower than in the tank, but higher than the ambient temperature, despite having a well-mixed temperature distribution before nightfall. This suggested that reverse flow occurred and Tang *et al.* [24, 25] discovered that this reverse flow is highly dependent on the tilt angle of the evacuated tubes. But the effect of reverse flow has no significant impact on any heat loss of the ETSC during the night. An important point that can be taken out from those research studies is that thermal stratification within an ETSC is highly dependent on the inclination of the evacuated tubes.

4. Experimental Setup

The methodology consists of conducting an experimental study on a passive water-in-glass ETSC and validating a 3D numerical model with the collected data. Once the numerical model validated, the novel ETSC can then be investigated for improved energy capture.

The installation requirements of the available equipment and measuring instruments were in accordance with ISO 9806:2013. However, for simplification of the experimental exercise, as well as the numerical studies to be performed, the experiment was set up to evaluate the ETSC on a passive operation, with no water charge or discharge.

The installed ETSC at the University of Mauritius consists of 10 evacuated tubes, 21 mm apart, with a diameter of 57.8 mm and length of 1690 mm. The water tank has a diameter and length of 480 mm and 955 mm respectively, with a 50 mm layer of insulation. The evacuated tubes were set at 40° to the horizontal, according to the manufacturer's specification. No reflecting plate was used with the ETSC. Further details of the ETSC specifications are given in Appendix B, Table A.1.

Two Onset 12-Bit temperature smart sensors (model: S-TMB-002) were used for temperature measurements, connected to an Onset HOBO data logger station (model: H21-USB). The temperature sensor $T1$ was inserted through the pressure relief hole on top of the water tank, immersed 63.333 mm into the water, and $T2$ through the middle of the three water outlets from the bottom, immersed 126.667 mm into the water. Both $T1$ and $T2$ were found to be in the middle of the water tank from a side perspective (looking at the YZ plane in Figure 4). This was to avoid any unnecessary drilling or permanent modifications of the water tank. Figure 3(a) is a schematic representation of the experimental setup. As for the weather data, a Davis Instruments Vantage Pro Weather Station was used to capture ambient temperature, humidity, barometric pressure, wind speed, and solar irradiance on an inclined plane of 40° to the horizontal.

The experiment was carried out at the roof top of the Mechanical Workshop, Faculty of Engineering, Phase I Building, University of Mauritius in Reduit, Mauritius (20°14'09.4"S, 57°29'49.3"E, 318 m above sea level). The water tank of the ETSC was filled up with tap water in the morning before starting the measurements. The passive experiment was then left to run from 19.09.17 at 3:00pm to 03.10.17 at 3:00pm (a complete fortnight), after which the recorded values (temperatures and solar irradiance) were extracted and a 3-hour interval was selected for validation of the numerical model.

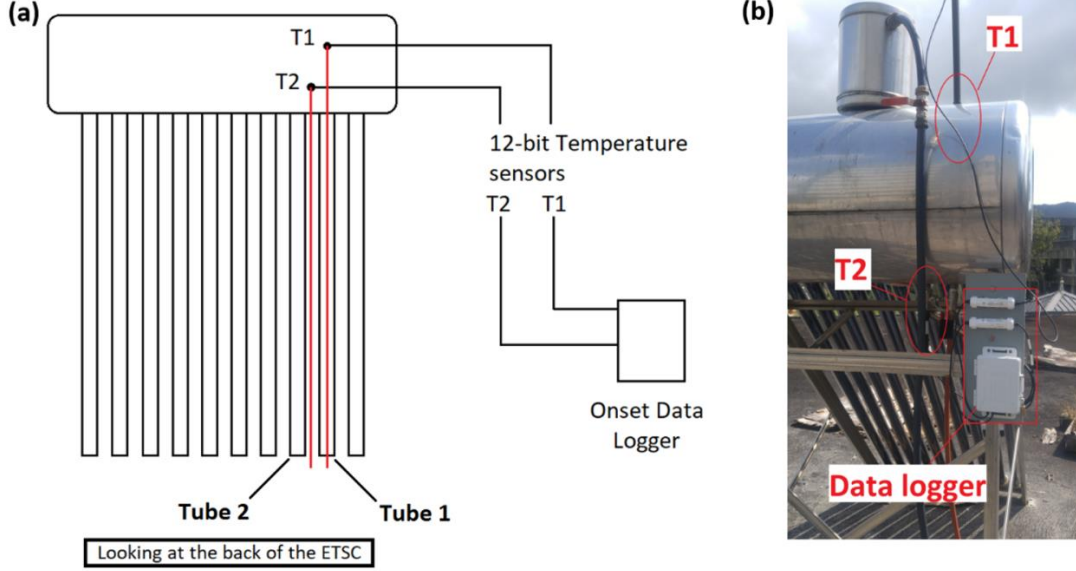


Figure 3 – (a): Schematic diagram of the experimental setup with temperature sensors T1 and T2. (b): Experimental setup showing positioning of the temperature sensors T1 and T2, and the data logger station.

5. Numerical Model

5.1. Governing Equations

For the numerical analysis, the commercial computational fluid dynamics software package Ansys Fluent 18.2 was used. The governing equations employed for this particular case are the continuity, momentum, and energy equations (Equations 1, 2 and 3 respectively) for a laminar flow and incompressible Newtonian fluid. To incorporate the buoyancy driven force due to small variations in water density because of an expected temperature gradient, the Boussinesq approximation model was employed. In this model, all water properties are considered to be constant, except for its density in the momentum source term which was subjected to temperature changes.

$$\frac{\partial u_i}{\partial x_i} = 0 \quad (1)$$

$$\rho' \left(\frac{\partial u_i}{\partial t} + \frac{\partial u_i u_j}{\partial x_j} \right) = - \left(\frac{\partial p}{\partial x_i} \right) + \mu \left(\frac{1}{3} \frac{\partial^2 u_j}{\partial x_i \partial x_j} + \frac{\partial^2 u_i}{\partial x_i \partial x_j} \right) + (\rho - \rho') g \quad (2)$$

$$\rho' \left(\frac{\partial h_{tot}}{\partial t} + \frac{\partial h_{tot} u_i}{\partial x_i} \right) - \frac{\partial p}{\partial t} = k \frac{\partial T}{\partial x_i \partial x_j} \quad (3)$$

where $h_{tot} = h + \frac{1}{2}\|u\|^2$ evaluates the total enthalpy of the domain, with ρ' being a reference density. The momentum source term is equated as $-\rho'\beta(T - T')g$, with T' as a constant reference temperature set to 310.32 K for all simulations [22]. The reference density was set to water density at 310.32 K and 101.325 kPa.

5.2. Domain Discretization

Only the occupied space by the water within the SWH was modelled, with the prolongations of the evacuated tubes within the water tank disregarded. To reduce the numerical demand because of limited computational resources (Intel® Core i7-6700 3.4GHz, 16.0GB RAM) and a short project timeframe, the computational domain considered was reduced to include only part of the SWH as shown in Figure 4. The red circles indicate the positions of the temperature sensors as used for the experiment.

The domain was then discretized with hexahedral cells, having a maximum aspect ratio of 13.82 and minimum orthogonality of 0.713 (Figure 5). A base simulation was carried out for the grid sensitivity study. The boundary conditions were taken as illustrated in Figure 6. It was concluded that a mesh of 103,118 hexahedral cells resulted in mesh-independent solutions at a timestep of 0.1 s. There was no significant effect on the solutions at lower timestep sizes.

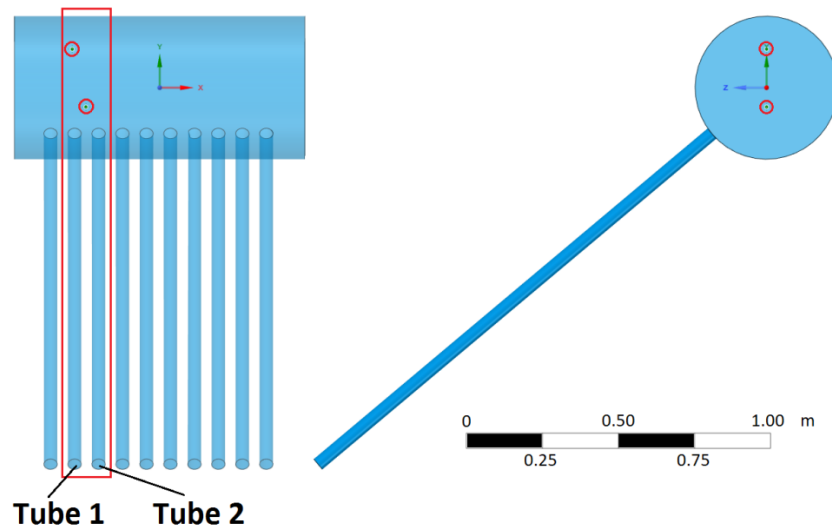


Figure 4 – The computational domain considered is sectioned as indicated by the red rectangle.

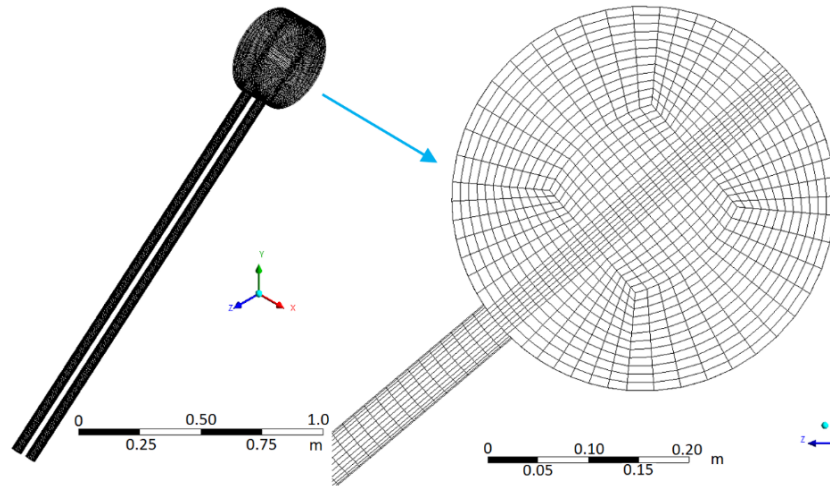


Figure 5 – Domain discretization with hexahedral cells.

5.3. Boundary and Initial Conditions

Thermal input contributed by the solar radiation was approximated for only the upper halves of the domain contained within the evacuated tubes. This energy input was considered to be as time-dependent, taken from a selected interval of the weather data obtained. An effective transmissivity-absorptivity product, $(\overline{\tau\alpha})$, of 0.86 was accounted with the heat input. As for any heat losses to the ambient, a global heat transfer coefficient of $0.6 \text{ W/m}^2\text{K}$ (as suggested by the manufacturer) was set for the entire domain, except for the symmetry region (Figure 6). The entire domain had a no-slip wall boundary condition imposed.

As for the initial conditions, the water was assumed to be in a stationary flow field as well as having a uniform temperature field before any heat flux is applied. The initial temperature was taken from the weather data at the start of the chosen interval. To account for the hydrostatic pressure within the SWH, the lowest node of the computational domain was taken as reference point at which its hydrostatic pressure was calculated. Gravity was considered to be in the negative y-direction (Figure 6), and the geometrical model set at 40° below the z-axis.

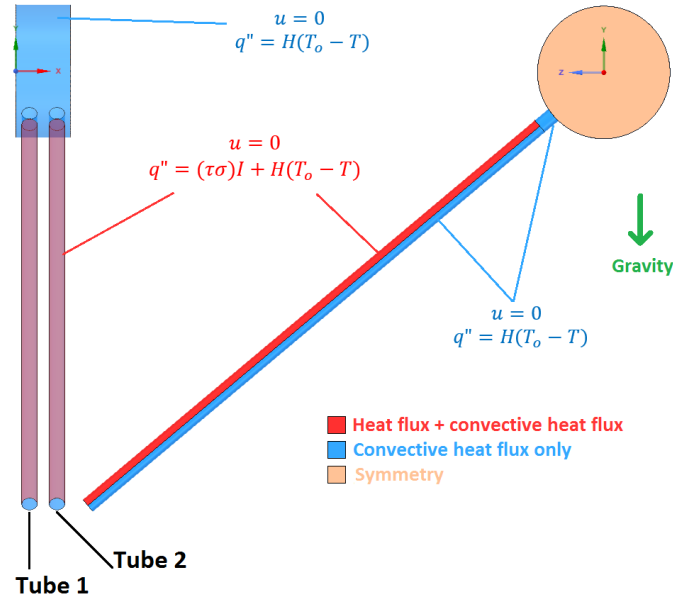


Figure 6 – Boundary conditions employed for all simulations.

5.4. Experimental Data and Validation

The recorded experimental values from the temperature sensors $T1$ and $T2$, as well as the ambient temperature, T_o , are illustrated in Figure 7. The values were taken over a period of 14 days, for intervals of 60 s. Similarly, the solar irradiance measurement from the weather data is plotted in Figure 8, along with the product of the recorded solar irradiance and the effective transmissivity-absorptivity product, $I(\overline{\tau\sigma})$. It can be noted that any rise and fall in temperatures $T1$, $T2$, and T_o , corresponds to the similar trends observed for the solar irradiance, as would be expected.

For the validation of the numerical model, only a selected 3-hour interval was chosen, which was data 20.09.17 as from 08:00am to 11:00am. Those times correspond to values recorded for the interval between 61,200 s to 72,000 s from Figures 7 and 8. The values of the ambient temperature and the calculated heat flux input, $I(\overline{\tau\sigma})$, for this particular interval are illustrated in Figure 9. Those two profiles are employed as their respective boundary conditions for validation of the numerical model.

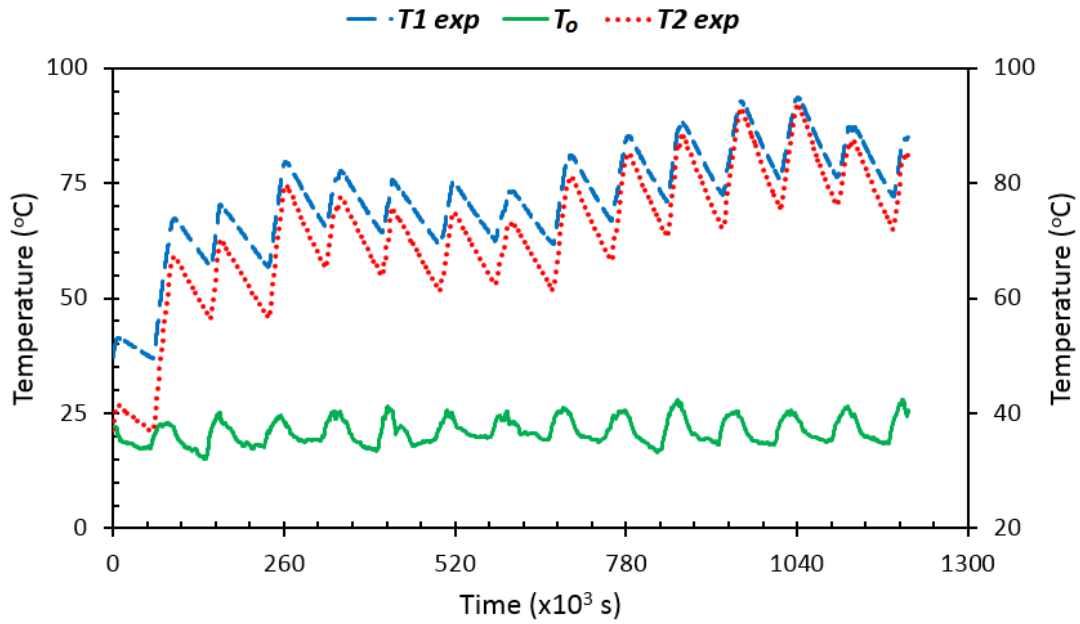


Figure 7 – Measured temperatures T1, T2, and T_0 , during the experiment. T1 and T_0 are referenced to the scale of the left, while T2 to that on the right.

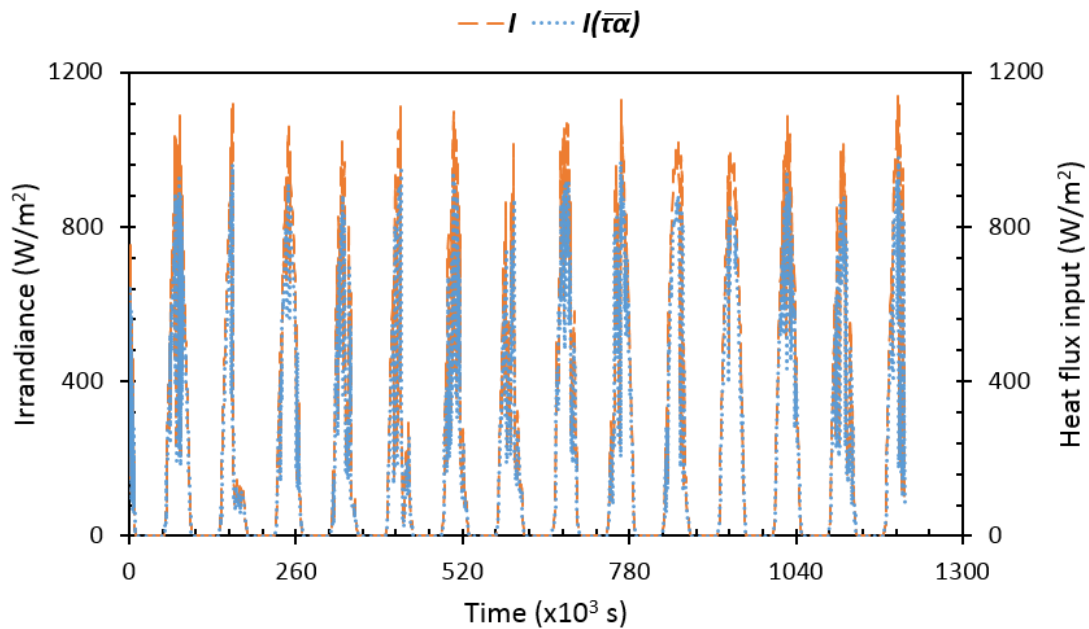


Figure 8 – Measured irradiance, I , during the experiment, and the calculated heat flux absorbed by the ETSC, $I(\tau\alpha)$. I is referenced to the scale of the left, and $I(\tau\alpha)$ to that on the right.

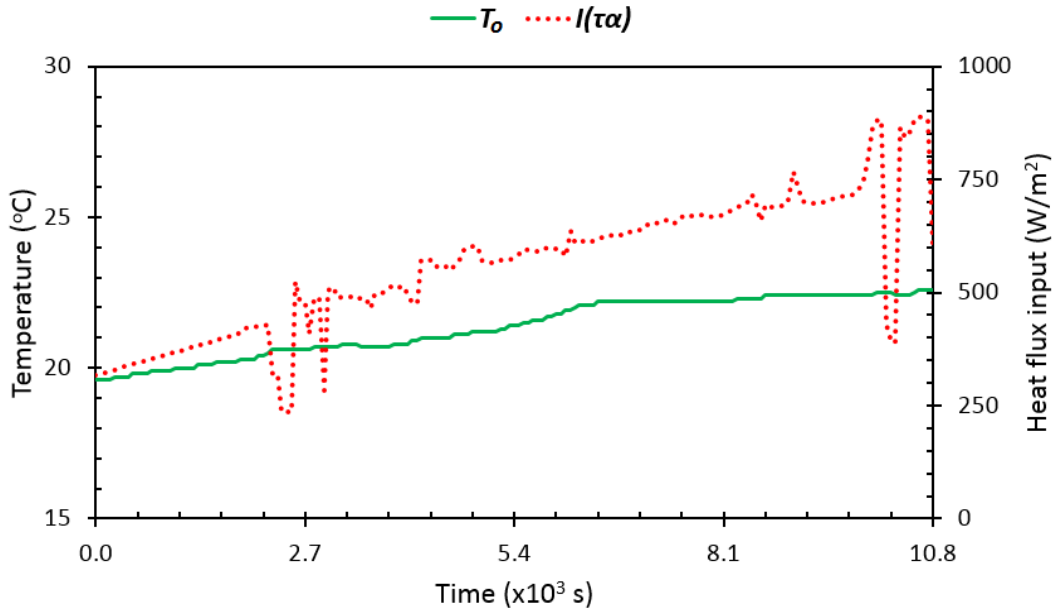


Figure 9 – Ambient temperature and heat flux input profiles employed as thermal boundary conditions for the numerical model. T_o is referenced to the scale of the left, and $I(\overline{\tau\alpha})$ to that on the right.

6. Results and Discussions

6.1 Validation of Numerical Model

The experimental data were compared with the simulated results as shown in Figure 10. It can be concluded that the developed numerical model in ANSYS Fluent shows good agreement with the experimental readings. $T1e$ and $T2e$ represents the data collected from the temperature sensors T1 and T2 respectively, and as for $T1s$ and $T2s$, they are the respective data points from the simulation data. The highest deviation noted was 2.06% and 1.89% for $T1$ and $T2$ respectively. The numerical errors can be explained through the simplification considered for the numerical model; the upper half area of the tube receiving the heat flux, overlooking any shadow of a tube cast on the other. This may explain the overestimation of the temperatures recorded from the numerical calculations. Nevertheless, the numerical model can be considered to be suitable for investigating the dynamic and thermal behaviour of the studied SWH.

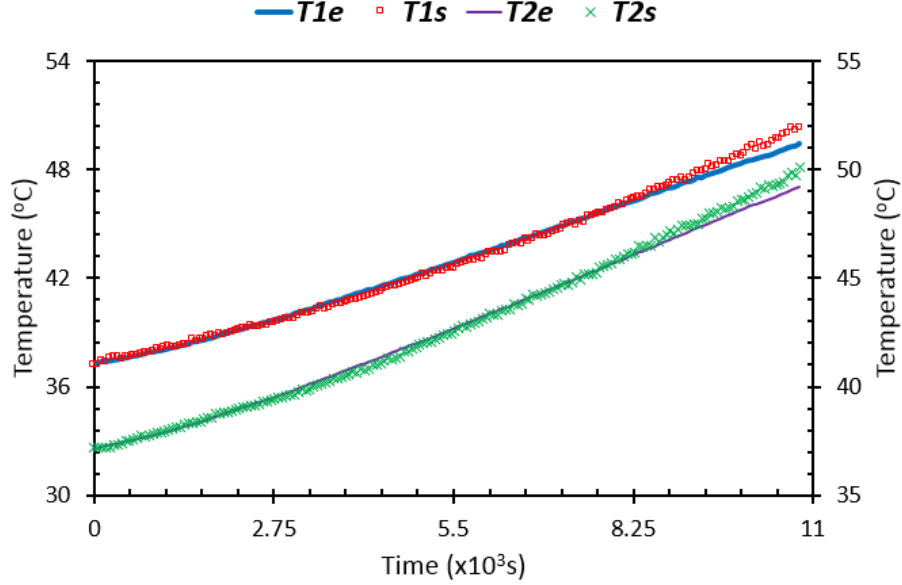


Figure 10 – Validation of the numerical model by comparing temperature readings from sensors T1 and T2 to their corresponding points from the numerical calculation.

6.2 Temperature Fields

Figure 11 depicts the temperature contours of the SWH at 1 hour intervals. As can be observed, temperature mixing throughout the SHW is quite uniform in the water tank. However, a more pronounced temperature gradient was apparent within the evacuated tubes. This is due to the solar irradiance assumed to be applying on the upper half of the evacuated tubes and as a consequence the dual stream of hot and cold water arising from the buoyancy effect. The increase in temperature was about 5.0°C for each 1-hour exposure to the sun.

6.3 Thermal Efficiency of SWH

The thermal efficiency, η_T , of the SWH can be easily calculated through Equations 4 and 5. The total internal energy, E , of the numerical domain was determined through Equation 4.

$$E = \int_V \rho e dV \quad (4)$$

With the energy input being defined by the solar irradiance (with the effective transmissivity-absorptivity product accounted for), $I(\bar{\tau}\bar{\alpha})$, and the area of the evacuated tubes exposed to the solar irradiance, A_c , the thermal efficiency is given by Equation 5. Table 1 summarises the thermal

efficiency of the numerical domain. An overall thermal efficiency of 40.39% was calculated for an exposure of 3 hours following the trend of heat flux presented in Figure 9.

$$\eta_T = \frac{\Delta E}{I A_c} \tag{5}$$

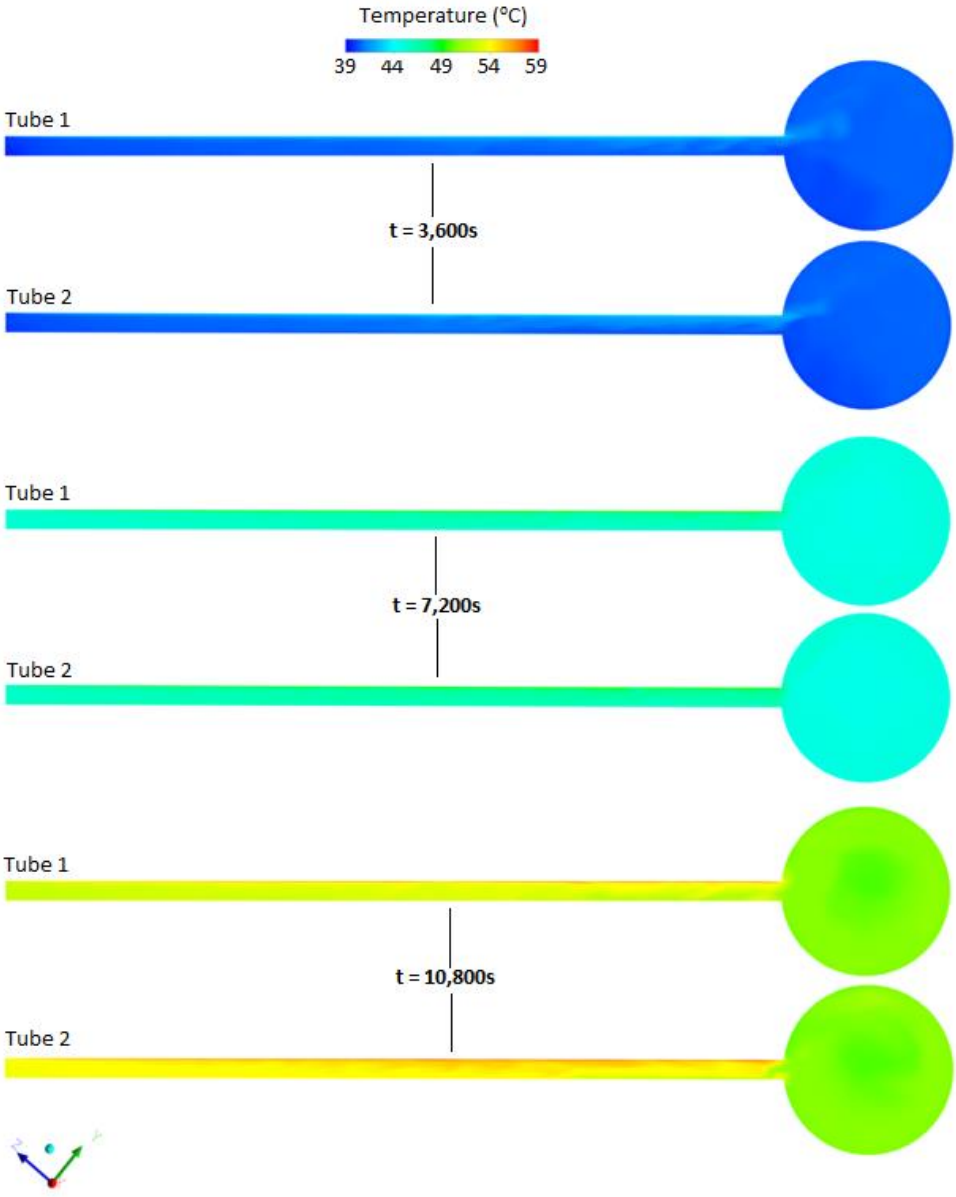


Figure 11 – Temperature contours for the SWH at 40° inclination at 1 hour intervals.

Table 1 – Overall thermal efficiency of the SWH as per results from the simulations after 3 hours of sun exposure.

Duration (s)	Solar energy input, IA_C , (J)	Difference in total internal energy, ΔE , (J)	Thermal efficiency, η_T , (%)
10,800	1,374,251	1,321,178	40.39

The trend for evolution of thermal efficiency with time for the 3 hours is presented in Figure 11. A relatively stable around 40.50%. However, whenever there is a fluctuation in solar irradiance, drastic changes in thermal efficiency of the SWH can be observed accordingly. The results suggest that the SWH becomes more efficient when operating at higher solar irradiance values. However, above 750 W/m^2 , there are only slight increases in thermal efficiency for a big increase in solar irradiance. In a practical sense, it can be concluded that operating within $500 - 800 \text{ W/m}^2$ can be considered as being the optimal operating range. Any further increase in solar irradiance will only result in a very low, if not insignificant, increase in thermal efficiency.

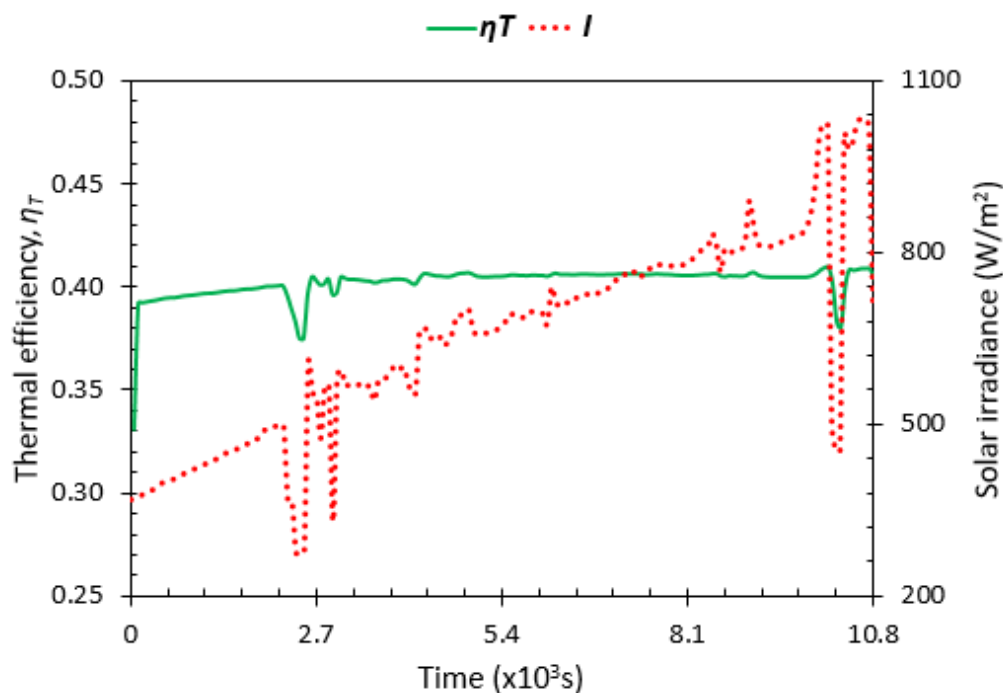


Figure 12 – Time evolution of solar flux input and thermal efficiency of the SWH. η_T is referenced to the scale of the left, and I to that on the right.

Although, it is to be noted that the overall thermal efficiency calculated above is referenced to the partial computational domain considered. The actual overall thermal efficiency of the installed

SWH may be by a small amount, but not far from what has been simulated. If the entire SWH was considered for the simulation, the number of sections of the computational domain will be multiplied by the same factor of the solar energy supplied, except for a relatively small discrepancy when accounting for the side ends of the SWH. This will therefore result in a somewhat slightly different overall thermal efficiency as obtained.

6.4 Effect of Tube Diameter on Thermal Efficiency

With the thermal numerical model devised validated, further studies were performed. The diameter of the evacuated tubes was varied to investigate its effects on the thermal efficiency of the SWH. The actual tube dimensions are 44.0 mm in internal diameter, with an external diameter of 57.8 mm, and 1,690 mm in length. The spacing between the evacuated tubes are 21.0 mm, with a distance of 767.0 mm from one extremity of the tubes to the other. The SWH was manufactured with a total number of 10 evacuated tubes. To bring this analysis a comparative one, a dimensionless value, D^* , is employed (Equation 6). This results in the current D^* value to be 2.752. Note that the external diameter, the number of and the spacing between the evacuated tubes evacuated tubes, were all three kept constant. This way the only variance considered is the global collector area of exposure, i.e. the amount of water being exposed to the solar irradiance (Figure 2b).

$$D^* = \frac{\text{internal diameter of evacuated tube}}{\text{spacing between evacuated tubes}} \quad (6)$$

The considered D^* were 1.75, 2.095, and 2.25. Table 2 summarize the dimensions as a results of the proposed D^* values.

Table 2 – Variation in internal tube diameter as a result of changes in D^* .

D^*	Internal tube diameter (mm)
1.750	36.75
2.095	44.00
2.250	47.25

With those new dimensions, the same numerical model and boundary and initial conditions were employed to evaluate the effect of varying the internal tube diameters on the thermal efficiency of

the SWH. The results for the time evolution of the SWH thermal efficiency is illustrated in Figure 13.

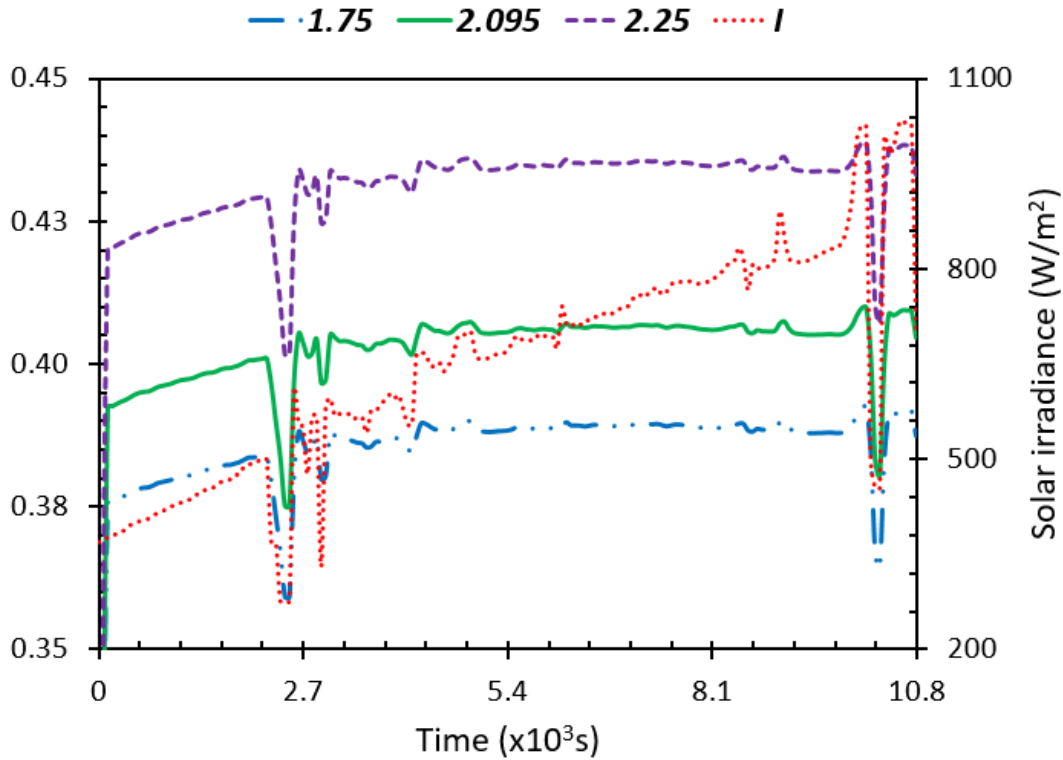


Figure 13 – Time evolution of thermal efficiency of the SWH and solar flux input. η_T is referenced to the scale of the left, and I to that on the right.

A noticeable increase in thermal efficiency is noted for increasing inner diameter of the evacuated tubes. This is related to the increase in surface area that is exposed to the solar irradiance as well as a bigger volume of water contained within the tubes, given that the heat loss to the environment stays the same, having considered no changes in material properties. It is also worth noticing that an increase in inner diameter of the evacuated tubes demonstrate no effect on the thermal efficiency pattern with similar solar irradiance.

6.5 Effect of Climatic Conditions on Thermal Efficiency

The changes in climatic conditions have been known to be very impactful on the performance of a SWH. For example, a reduction in solar irradiance due to cloudy weather, during rainfall, or during a windy day [23, 24, 26]. To make the study more relevant to the climatic conditions of Mauritius, the thermal efficiency of the SWH was investigated with varying solar irradiance from data obtained at three different locations: Port Louis, Reduit, and Curepipe, each exhibiting its

respective solar irradiance input for a period of 3 hours at the same day time, i.e. from 09:00 am to 11:00 am. The results are illustrated in Figure 14.

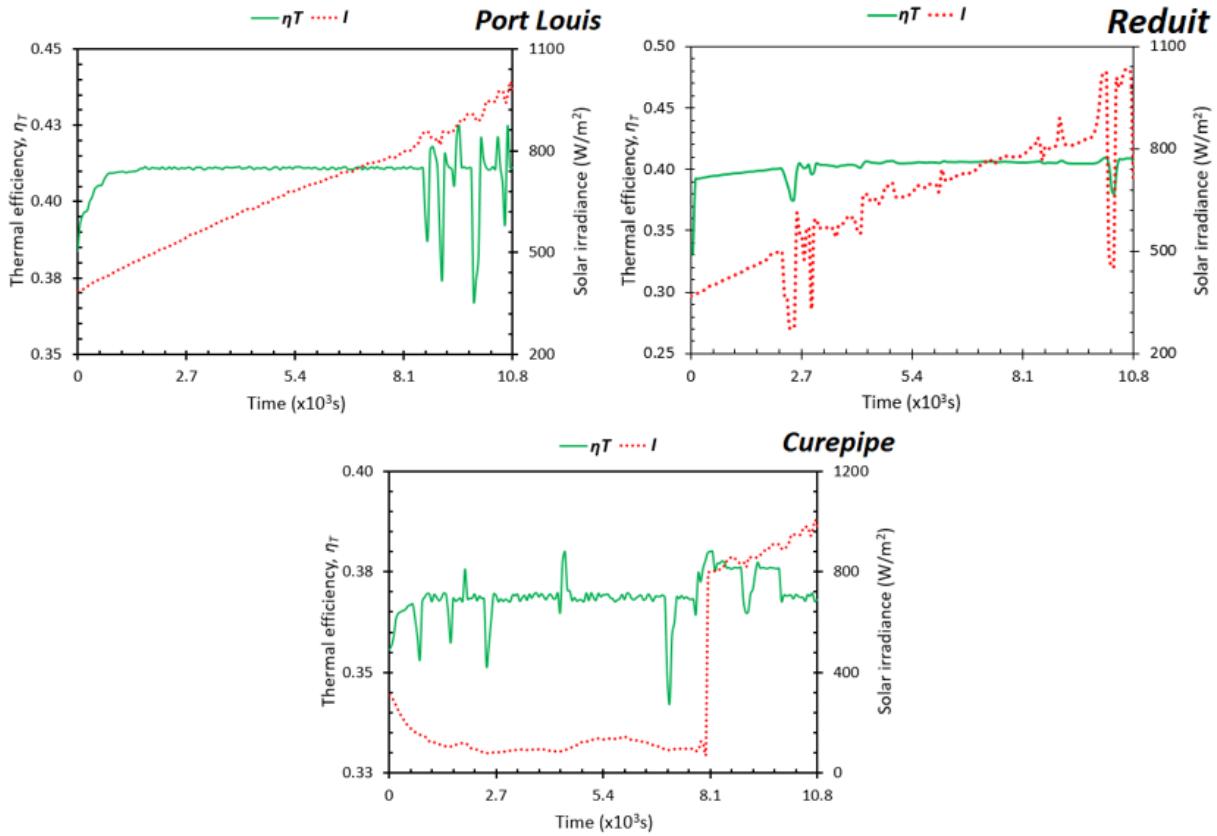


Figure 14 – Time evolution of thermal efficiency of the SWH and solar flux input. η_T is referenced to the scale of the left, and I to that on the right. (a): Port Louis region, (b) Reduit region, (c): Curepipe region.

The solar irradiance increases almost linearly until the 8.10×10^3 s time mark is reached, which then becomes quite erratic. This is quite common for the region as Port Louis experiences more sunshine as compared to other regions of the island. For the region of Reduit, the solar irradiance shows some erratic behaviours, but nevertheless with an increasing trend, which can be explained by the passage of frequent clouds from time to time. And when considering a region on the central plateau, where rainy and cloudy days are frequent, the solar irradiance is significantly lower for more than the first two hours.

It was observed that the thermal efficiency is slightly affected by a significant difference in solar irradiance level. The thermal efficiency increases with higher solar irradiance values, but even so slightly, until it reaches to a point where any further increase in solar irradiance will result in an

insignificant increase in thermal efficiency. The optimum operating range was found to be around 650 to 850 W/m².

Despite those differences in solar irradiance, the thermal efficiency was found to slightly vary within a certain range (around 40.00%). However, any irregular changes in the solar irradiance led to drastic decrease or increase in the thermal efficiency. This suggest that generally the thermal efficiency is susceptible to drastic changes in climatic conditions on a real-time basis, but remains unaffected if a constant or linear increment in solar irradiance is maintained.

It was calculated that the overall thermal efficiency values for the 3-hour duration were 41.00%, 40.50%, and 37.50% for the regions of Port Louis, Reduit, and Curepipe respectively. The thermal efficiency under the climatic conditions of Curepipe was significantly lower because of the unfavourable conditions during the first 2 hours of the simulation runtime.

7. Conclusion

An experiment was set up to collect relevant data for the validation of a numerical model on passive operation, where there is no charge and discharge of water. The three dimensional numerical model was developed and successfully validated with the experimental data in relevance to the tropical conditions of Reduit, Mauritius. Employing the Boussinesq's Approximation is a valid assumption for this particular case. At an inclination of 40°, when considering a solar irradiance profile obtained from 20.09.17 08:00am to 11:00am, an overall thermal efficiency 40.39% was calculated. It was also observed that a relatively well-mixed temperature profile was obtained at this particular tilt angle.

This numerical model can predict the thermal efficiency of a passively operating SWH. The effects of several features on the SWH thermal efficiency can be investigated through this thermal model. Such parameters can be the geometrical features of the evacuated tubes and water tank, the materials of which the SWH is made of, and the tilt angle of the SWH. It can also be adapted with recorded weather data obtained for a particular region for optimisation of the system.

References

1. Hussain, A., S.M. Arif, and M. Aslam, *Emerging renewable and sustainable energy technologies: State of the art*. Renewable and Sustainable Energy Reviews, 2017. **71**: p. 12-28.
2. Mohanty, S., et al., *Forecasting of solar energy with application for a growing economy like India: Survey and implication*. Renewable and Sustainable Energy Reviews, 2017. **78**: p. 539-553.
3. Kannan, N. and D. Vakeesan, *Solar energy for future world: - A review*. Renewable and Sustainable Energy Reviews, 2016. **62**: p. 1092-1105.
4. Hansen, J.P., P.A. Narbel, and D.L. Aksnes, *Limits to growth in the renewable energy sector*. Renewable and Sustainable Energy Reviews, 2017. **70**: p. 769-774.
5. Mussard, M., *Solar energy under cold climatic conditions: A review*. Renewable and Sustainable Energy Reviews, 2017. **74**: p. 733-745.
6. *Climate of Mauritius*. 2017 [cited 2017 20.09.2017]; Available from: <http://metsservice.intnet.mu/climate-services/climate-of-mauritius.php>.
7. Surroop, D. and P. Raghoo, *Energy landscape in Mauritius*. Renewable and Sustainable Energy Reviews, 2017. **73**: p. 688-694.
8. Ciriminna, R., et al., *Rethinking solar energy education on the dawn of the solar economy*. Renewable and Sustainable Energy Reviews, 2016. **63**: p. 13-18.
9. Suman, S., M.K. Khan, and M. Pathak, *Performance enhancement of solar collectors—A review*. Renewable and Sustainable Energy Reviews, 2015. **49**: p. 192-210.
10. Lin, W., W. Gao, and T. Liu, *A parametric study on the thermal performance of cross-corrugated solar air collectors*. Applied Thermal Engineering, 2006. **26**(10): p. 1043-1053.

11. Karsli, S., *Performance analysis of new-design solar air collectors for drying applications*. Renewable Energy, 2007. **32**(10): p. 1645-1660.
12. Chamsa-ard, W., et al., *Thermal Performance Testing of Heat Pipe Evacuated Tube with Compound Parabolic Concentrating Solar Collector by ISO 9806 - 1*. Energy Procedia, 2014. **56**: p. 237-246.
13. Buker, M.S. and S.B. Riffat, *Building integrated solar thermal collectors – A review*. Renewable and Sustainable Energy Reviews, 2015. **51**: p. 327-346.
14. Sabiha, M.A., et al., *Progress and latest developments of evacuated tube solar collectors*. Renewable and Sustainable Energy Reviews, 2015. **51**: p. 1038-1054.
15. Devecioglu, A.G. and V. Oruc, *Experimental Investigation of Thermal Performance of a New Solar Air Collector with Porous Surface*. Energy Procedia, 2017. **113**: p. 251-258.
16. Martinez, R.G., et al., *Performance assessment of an unglazed solar thermal collector for envelope retrofitting*. Energy Procedia, 2017. **115**: p. 361-368.
17. Bunea, M., et al. *Performance of solar collectors under low temperature conditions. in Measurements and simulations results*. 2012.
18. Morrison, G.L., I. Budihardjo, and M. Behnia, *Water-in-glass evacuated tube solar water heaters*. Solar Energy, 2004. **76**(1): p. 135-140.
19. Zhang, X., et al., *Experimental investigation of the higher coefficient of thermal performance for water-in-glass evacuated tube solar water heaters in China*. Energy Conversion and Management, 2014. **78**: p. 386-392.
20. Thant, Z.M., M.M. Soe, and M.M. Htay, *Numerical Study on Temperature Distribution of Water-in-Glass Evacuated Tubes Solar Water Heater*.
21. Thomas, D.E., *Perofrmance of Horizontal Water-in-Glass Evacuated Tube Solar Collectors*. Journal of Mechanical Engineering, 2017. **45**(2): p. 130-134.

22. Bracamonte, J., et al., *Effect of the collector tilt angle on thermal efficiency and stratification of passive water in glass evacuated tube solar water heater*. Applied Energy, 2015. **155**(Supplement C): p. 648-659.
23. Bracamonte, J., *Effect of the transient energy input on thermodynamic performance of passive water-in-glass evacuated tube solar water heaters*. Renewable Energy, 2017. **105**(Supplement C): p. 689-701.
24. Tang, R. and Y. Yang, *Nocturnal reverse flow in water-in-glass evacuated tube solar water heaters*. Energy Conversion and Management, 2014. **80**(Supplement C): p. 173-177.
25. Tang, R., Y. Yang, and W. Gao, *Comparative studies on thermal performance of water-in-glass evacuated tube solar water heaters with different collector tilt-angles*. Solar Energy, 2011. **85**(7): p. 1381-1389.

Appendix A

The features and characteristics of the solar water tank is detailed in the table below.

Table A. 1 – Geometrical features and characteristics of the installed solar water heater.

<i>Water Tank</i>	
<i>Material</i>	Stainless Steel 304-3B
<i>Length</i>	0.945 m
<i>Diameter</i>	0.038 m
<i>Thickness</i>	0.0004 m
<i>Insulating material thickness</i>	0.050 m
<i>Evacuated Tubes</i>	
<i>Material</i>	Borosilicate 3.3 Glass
<i>Length</i>	1.690 m
<i>Inner diameter</i>	0.044 m
<i>Thickness</i>	0.0016 m
<i>Absorber Coating</i>	
<i>Absorptivity</i>	0.92 – 0.96
<i>Emissivity</i>	0.0 – 0.08